Uplink Secrecy Performance of RIS-based RF/FSO Three-Dimension Heterogeneous Networks

Dawei Wang, Menghan Wu, Zhongxiang Wei, Keping Yu,
Lingtong Min, and Shahid Mumtaz

***Abstract*—In this paper, a novel reconfigurable intelligent surface (RIS)-assisted HAP-UAV secure multi-user mixed radio frequency (RF)/free space optical (FSO) system is proposed. Specifically, the Gamma-Gamma distribution is utilized to characterize the atmospheric turbulence effect for the FSO link from UAV to HAP, while the Rayleigh and Nakagami-m distribution fading are applied to simulate the legitimate and wiretap RF links, respectively. We present the closed-form expressions for the probability density functions, the cumulative distribution functions, and the secrecy outage probability (SOP) of the end-to-end signal-to-noise ratio (SNR) in terms of Meijer's G-function. To gain more insight into secrecy performance, we further obtain the closed-form expressions for the asymptotic SOP, the asymptotic probability of positive secrecy capacity (PPSC), the diversity gain, and the coding gain at high SNR regions. We can observe that the secrecy performance depends on the weaker channel between the RF and FSO, and is closely related to the number of RIS elements, the number of terrestrial users, the atmospheric turbulence factor, pointing error parameters, and the fading parameter of Nakagami-m distributed wiretap link. Finally, numerical results validate the derived results and demonstrate that the proposed design achieves superior secrecy performance over the benchmarks.**

***Index Terms*—Heterogeneous HAP/UAVs networks, reconfigurable intelligent surface, mixed RF/FSO uplink channel, secrecy outage probability.**

I. Introduction

High-altitude platform (HAP) and unmanned aerial vehicles (UAVs) heterogeneous networks enable three-dimensional (3D) broadband connectivity for sixth-generation (6G) communications [1], [2]. HAP and on-demand deployment of UAVs hovering at low altitudes [3], provide fast deployment, wide coverage, and low-cost communication mechanisms, particularly suitable for serving rural areas and disaster sites where terrestrial communications are unavailable [4]. Typically, mixed radio frequency (RF)/free space optical (FSO) transmission is deployed to serve HAP and UAV heterogeneous networks, due to its advantages on ultra-high data rates, license-free spectrum, and FSO's high-security [5]. It lets ground users transmit signals to the UAV via the RF link, where the optical signal is produced by transforming the electrical signal and then forwarded to the HAP via the FSO link [6].

Wireless RF communication is bound to be accompanied by information leakage due to its broadcast nature [7]. From that, academics have conducted a great deal of research on physical-layer security (PLS). [8]. By taking use of the channel spatiality, PLS aims to improve the quality of communication on legitimate links while decreasing it on wiretap links [9]. However, due to the low number of antennas at users and UAVs, secure beamforming is generally achieved with the help of an external enabler, such as a low-cost passive reconfigurable intelligent surface (RIS) [10]. It actively changes the direction of signals and achieves in-phase superposition, guaranteeing high secrecy performance for the RF link [11].

A. Related Works

Numerous researches have examined the effectiveness of mixed RF/FSO systems. Multi-user downlink performance of the asymmetric RF/FSO link was investigated in [12], where the satellite delivered a signal to a UAV through an FSO link, and the users received the signal forwarded by the UAV through the RF. Lin $et\ al.$ derived the moment generating function, probability density function (PDF), and cumulative distribution function (CDF) of instantaneous SNR [13]. The authors in [14] modeled the FSO channel by considering the pointing errors (PEs) and then presented the outage probability (OP), average bit error probability, etc. In [15], the RF/FSO satellite system was investigated, where the RF or FSO links were selected based on the weather condition. Then the authors obtained the OP expressions and the asymptotic outage probability for this weather-aware system. In [16], the authors incorporated non-orthogonal multiple access (NOMA) in mixed RF-FSO networks, where the pointing errors and Gamma-Gamma turbulence are present on FSO backhaul link.

On the topic of security issue with mixed RF/FSO links, the security-reliability trade-off (SRT) is a key point investigated

This work was supported in part by the National Natural Science Foundation of China under Grant 62271399 and 62206221, in part by the Key Research and Development Program of Shaanxi Province under Grant 2022KW-07, in part by National Key Research and Development Program of China under Grant 2020YFB1807003, and in part by Foundation of the Science, Technology, and Innovation Commission of Shenzhen Municipality under Grant JCYJ20190806160218174. *(Corresponding author: Lingtong Min; Zhongxiang Wei; Keping Yu)*

Dawei Wang, Menghan Wu, and Lingtong Min are with the School of Electronics and Information, Northwestern Polytechnical University, Xi'an, Shaanxi, 710072, China. They are also with the Research & Development Institute of Northwestern Polytechnical University in Shenzhen, Shenzhen, Guangdong, 518057, China (e-mail: wangdw@nwpu.edu.cn; 2021202128@mail.nwpu.edu.cn; minlingtong@nwpu.edu.cn)

Zhongxiang Wei is with the College of Electronic and Information Engineering, Tongji University, Shanghai 201804, China (e-mail: z_wei@tongji.edu.cn).

Keping Yu is with the Graduate School of Science and Engineering, Hosei University, Tokyo 184-8584, Japan (email: keping.yu@ieee.org).

Shahid Mumtaz is with the Department of Applied Informatics Silesian University of Technology Akademicka 16 44-100 Gliwice, Poland and is also with Department of Engineering, the Nottingham Trent University, Uk (e-mail: Dr.shahid.mumtaz@ieee.org).

in communication society. The authors in [17] investigated an cooperative energy-harvesting cognitive source and several eavesdroppers (Eves), where the SRT is used to measure the performance of the relay selection schemes. Bin *et al.* analyzed the SRT in the wireless sensor network by constructing the outage and wiretap probability equations [18], where several multiple access strategies were adopted to enhance the PLS performance. Secrecy outage probability (SOP) and the probability positive secrecy capacity (PPSC) are other widely used metrics for measuring secrecy performance. Researchers in [19] presented a frequency-domain strategy to evaluate both the SOP and PPSC based on the moments generating function (MGF). Authors in [20] analyzed the PPSC in hybrid FSO and millimeter wave (mmWave) wiretap systems for different types (FSO-only, mmWave-only, and hybrid) of Eves. Eylem *et al.* studied the SOP and PPSC performance while taking RF and FSO attacks into account. The Nakagami-m is modeled for RF link and exponentiation Weibull is modeled for FSO link [21]. In [22], collusion and non-collusion Eves are taken into account in the investigation of a dual-hop mixed RF/FSO communication system with diversity combining techniques. Additionally, in terms of Meijer's G function, the lower bound for SOP and effective secrecy throughput (EST) has been derived.

As a promising PLS enhancement technology, the performance of RIS-aided secure communication has also been extensively analyzed. In [23], the authors derived the exact SOP and EST for the RIS-assisted NOMA downlink networks, where both external and internal eavesdroppers were considered. Ping *et al.* investigated the PDF and CDF of the end-to-end SNR for the RIS-aided system [24]. The authors in [25] studied the NOMA-aided transmitting and maximized the security rate by jointly optimizing transmit power and phase shifts of the RISs.

B. Motivations and Contributions

While extensive research has been conducted for RF/FSO networks in terms of channel modeling and performance analysis [12]–[16], the security of mixed RF/FSO systems is not well studied. Several papers have investigated the system secrecy performance by studying the SRT, SOP, average secrecy capacity (ASC), ASC, and PPSC [17], [18], [20]–[22], but they lack the safety enhancement of the vulnerable RF links.

Motivated by the above, we propose a RIS-assisted HAP-UAV heterogeneous framework for achieving high-rate, reliable but secure communications in this paper. To our best knowledge, this is the first study on the secrecy performance analysis of a mixed RF/FSO HAP-UAV system with the assistance of the RIS. The main contributions are summarized as below.

- First, we present a novel RIS-assisted mixed RF/FSO HAP-UAV heterogeneous multi-user system, where the Gamma-Gamma, Rayleigh, and Nakagami-m distributions are used to model the mixed RF/FSO channels.
- Second, we investigate PDFs and CDFs of end-to-end SNRs, including the legitimate RF link from the user to the UAV, the legitimate FSO link from the UAV to the HAP, as well as the wiretap RF link from the users to the Eve. Then we further obtain the closed-form expressions for SOP in terms of Meijer's G-function.
- Finally, to gain more insights, we study the asymptotic SOP, PPSC, system diversity order, and coding gain at high SNR regions. Both theoretical and simulation results indicate that the number of users, RIS elements, and FSO fading factors are critical to secrecy performance.

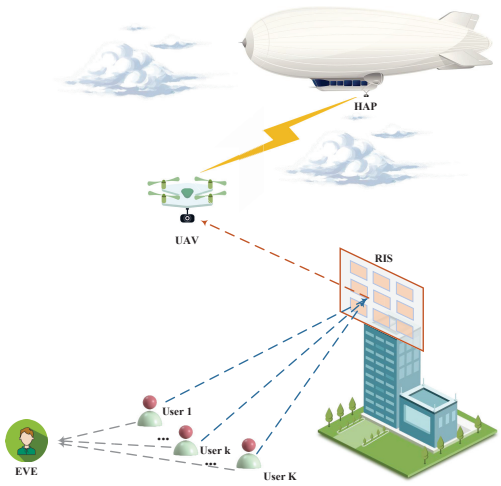

Fig. 1. A sketch of secure RIS-based FSO/RF two-layer heterogeneous networks

The remainder of this paper is as follows. Section II describes the channel model for both RF and FSO links. The secrecy performance analysis is shown in Section III, where the end-to-end statistical characteristics, such as SOP and asymptotic SOP are obtained. Section IV presents extensive simulations, and Section V concludes the paper.

II. System and Channel Model

A RIS-based RF/FSO two-layer heterogeneous network is shown in Fig. 1. There are K terrestrial users denoted as $\mathbb{S} = \{s_1, ..., s_K\}$, where users (S) transmit confidential information to the UAV (U) with the assistance of a RIS (R) via the RF link. Then, the UAV decodes electrical signals into optical signals and forwards them to the HAP (D) in the FSO link subsequently [26]. There is a passive Eve (E) attempting to intercept confidential data from the users. Note that, the security issue of the FSO link is naturally guaranteed due to its narrow and undetectable laser beam.

A. RF Channel Model

1) RF Channel Model between S→U: We adopt the opportunistic scheduling policy for the user selection. According to the SNR of the S→U links, the users with the largest SNR is scheduled for data transmission. Assuming that the k-th user is scheduled and the received signal at UAV can be written as [27]

$$y_{k,U} = \sqrt{P_S}\left(\mathbf{h}_{R,U}^{k}\right)^{H} \mathbf{\Theta} \mathbf{h}_{S,R}^{k} x_S^k + n_U, \tag{1}$$

where P_S is the k-th user's transmission power, x_S^k is the k-th user's transmitted signal with unit energy, and n_U is the AWGN with zero mean and power spectral density $N_{0,u}$. The RIS has N passive reflecting elements with phase $\mathbf{\Theta} = \text{diag}\left(e^{j\theta_1}, e^{j\theta_2}, ..., e^{j\theta_N}\right)$, where $\theta_n \in (0, 2\pi]$ is the phase shift coefficient of the n-th RIS reflecting element. The matrix $\mathbf{h}_{R,U}^k$ and $\mathbf{h}_{S,R}^k$ represent the complex channel coefficients from RIS to the UAV and from k-th user to the RIS, respectively. The channel vectors can be written as $\mathbf{h}_{R,U}^k = \left\{h_{R,U}^{k,1}, h_{R,U}^{k,2}, ..., h_{R,U}^{k,N}\right\} \in \mathbb{C}^{1\times N}$ and $\mathbf{h}_{S,R}^k = \left\{h_{S,R}^{k,1}, h_{S,R}^{k,2}, ..., h_{S,R}^{k,N}\right\} \in \mathbb{C}^{1\times N}$, where $h_{S,R}^{k,n} = \left|h_{S,R}^{k,n}\right| e^{j\varphi_{n,k}}$ and $h_{R,U}^{k,n} = \left|h_{R,U}^{k,n}\right| e^{j\phi_{k,n}}$, $\varphi_{n,k}$, $\phi_{k,n} \in (0, 2\pi]$ are the phase shift coefficient of the subchannels, $n \in \mathbb{N} = \{1, 2, ..., N\}$. Therefore, the SNR at the UAV is calculated as

$$\tilde{\gamma}_{k,U} = \frac{P_S}{N_{0,u}} \left| \sum_{n=1}^{N} \left|h_{R,U}^{k,n}\right| \left|h_{S,R}^{k,n}\right| e^{j\phi_{k,n}+\theta_n+\varphi_{k,n}} \right|^2. \tag{2}$$

Considering the optimal phase shift $\theta_n^* = -\left(\phi_{k,n} + \varphi_{k,n}\right)$ [28], the maximum $\tilde{\gamma}_{k,U}$ can be achieved as

$$\gamma_{k,U} = \bar{\gamma}_{S,U} \left| \sum_{n=1}^{N} \left|h_{R,U}^{k,n}\right| \left|h_{S,R}^{k,n}\right| \right|^2, \tag{3}$$

where $\bar{\gamma}_{S,U} = \frac{P_S}{N_{0,u}}$ denotes the average SNR. The terms $h_{R,U}^{k,n} \sim \mathcal{CN}\left(0, d_{R,U}^{-2}\right)$ and $h_{S,R}^{k,n} \sim \mathcal{CN}\left(0, d_{k,R}^{-2}\right)$ are both Rayleigh random variables (RVs) with zero mean and variances $d_{R,U}^{-2}$ and $d_{k,R}^{-2}$, where $d_{R,U}$ and $d_{k,R}$ are the communication distance between R→U and distance between s_k→R, respectively.

Lemma 1. *the PDF and CDF of $\gamma_{k,U}$ can be derived as*

$$f_{\gamma_{k,U}}(\gamma) = \frac{1}{2\Gamma(\eta)\lambda_k^{\eta}} \cdot \gamma^{\left(\frac{\eta-2}{2}\right)} \cdot \exp\left(-\frac{\sqrt{\gamma}}{\lambda_k}\right), \tag{4}$$

and

$$F_{\gamma_{k,U}}(\gamma) = 1 - \frac{1}{\Gamma(\eta)} \cdot \Gamma\left(\eta, \frac{\sqrt{\gamma}}{\lambda_k}\right), \tag{5}$$

where $\eta = \frac{N\pi^2}{16-\pi^2}$ and $\lambda_k = \frac{\sqrt{\bar{\gamma}_{S,U}}\left(16-\pi^2\right)}{4\pi d_{R,U} d_{k,R}}$ are the shape and scale parameter, respectively, $\Gamma(x)$ is the Gamma function, and $\Gamma(a, x)$ is the incomplete Gamma function. The above equations are accurately applied to arbitrary size N of RIS [29][1] □

Proof. Please see Appendix A. ■ □

2) RF Channel Model between S→E: The signal received at Eve from user k can be written as

$$y_{k,E} = \sqrt{P_S} h_{S,E}^k x_S^k + n_E, \tag{6}$$

where $h_{S,E}^k$ denotes the channel from the k-th user to Eve and $n_E \sim \mathcal{N}(0, N_{0,e})$ is the AWGN at Eve. The SNR at the Eve, defined as $\gamma_{S,E} = \bar{\gamma}_{S,E}\left(h_{S,E}^k\right)^2$, is assumed to follow a Nakagami-m fading distribution [30]. It is a versatile model capable of describing both slow and fast fading scenarios whose PDF and CDF are given as

$$f_{\gamma_{k,E}}(\gamma) = \frac{\left(\frac{m}{\bar{\gamma}_{S,E}}\right)^m \gamma^{m-1}}{\Gamma(m)} \exp\left(\frac{-m\gamma}{\bar{\gamma}_{S,E}}\right), \tag{7}$$

and

$$F_{\gamma_{k,E}}(\gamma) = 1 - \frac{1}{\Gamma(m)} \Gamma\left(m, \frac{m\gamma}{\bar{\gamma}_{S,E}}\right), \tag{8}$$

where m is the fading parameter, and $\bar{\gamma}_{S,E} = \frac{P_S}{N_{0,e}}$ is the average SNR.

B. FSO Channel Model

The optical signal received at the HAP is

$$y_{U,D} = \sqrt{P_U}\zeta h_{U,D} x_U + n_D, \tag{9}$$

where P_U is UAV's transmit power and x_U is the electrical signal transmitted by the UAV with unit energy. $n_D \sim \mathcal{N}(0, N_{0,h})$ is the AWGN at HAP and ζ is the electrical-optical conversion coefficient. The SNR at the HAP is defined as: $\gamma_{U,D} = \bar{\gamma}_{U,D}|h_{U,D}|^2$, where $\bar{\gamma}_{U,D} = \frac{P_U}{N_{0,h}}$ is the average SNR. Since $h_{U,D}$ depends on atmospheric turbulence (h_t), pointing errors (h_p), and path loss (h_l) caused by the random atmospheric radio medium, the FSO channel is given as

$$h_{U,D} = h_l h_p h_t. \tag{10}$$

The path loss h_l is determined by the distance from the UAV to HAP, expressed as[2]

$$h_l = \exp(-a d_{U,D}), \tag{11}$$

where a is the attenuation factor influenced by weather conditions. Pointing errors occurs when the transmitter aperture is not aligned with that of the receiver. The PDF of h_p can be written as [31]

$$f_p(h_p) = \frac{z^2}{A_0^{z^2}} h_p^{z^2-1}, \quad 0 \le h_p \le A_0, \tag{12}$$

where A_0 is a constant related to the pointing loss, and z represents the ratio between the equivalent beam width ω_{zeq} and the pointing error displacement standard deviation σ_z. In addition, we adopt Gamma-Gamma distribution to model h_t channel whose PDF can be expressed as [32]

$$f_{h_t}(h_t) = \frac{2(\alpha\beta)^{(\alpha+\beta)/2}}{\Gamma(\alpha)\Gamma(\beta)} h_t^{\frac{\alpha+\beta}{2}-1} K_{\alpha-\beta}\left(2\sqrt{\alpha\beta h_t}\right), \tag{13}$$

where $K_v(\cdot)$ is the modified Bessel function of the second kind of order (v). α and β are

$$\alpha = \left[\exp\left(\frac{0.49\delta_R^2}{\left(1 + 1.11\delta_R^{12/5}\right)^{7/6}}\right) - 1\right]^{-1}, \tag{14}$$

[1]Assessed by Kullback-Leibler divergence method, the difference between exact and approximate values is about 3.6×10^{-4}. Therefore it can be applicable to any size N.

[2]A 1550 nm wavelength for the fso channel is recommended due to its less path loss.

$$f_{\gamma_{U,D}}(\gamma)=\frac{z^2}{2\gamma\zeta\Gamma(\alpha)\Gamma(\beta)h_l^{z^2}}\left(\frac{\alpha\beta\sqrt{\gamma}}{A_0\sqrt{\bar{\gamma}_{U,D}}}\right)^{\frac{\alpha+\beta}{2}}G_{1,3}^{3,0}\left(\frac{\alpha\beta}{A_0h_l}\sqrt{\frac{\gamma}{\bar{\gamma}_{U,D}}}\,\middle|\,{}^{1+z^2-\frac{\alpha+\beta}{2}}_{z^2-\frac{\alpha+\beta}{2},\frac{\alpha-\beta}{2},\frac{-\alpha+\beta}{2}}\right), \tag{17}$$

$$F_{\gamma_{U,D}}(\gamma)=\frac{z^2}{\zeta\Gamma(\alpha)\Gamma(\beta)h_l^{z^2}}\left(\frac{\alpha\beta\sqrt{\gamma}}{A_0\sqrt{\bar{\gamma}_{U,D}}}\right)^{\frac{\alpha+\beta}{2}}G_{2,4}^{3,1}\left(\frac{\alpha\beta}{A_0h_l}\sqrt{\frac{\gamma}{\bar{\gamma}_{U,D}}}\,\middle|\,{}^{1-\frac{\alpha+\beta}{2},1+z^2-\frac{\alpha+\beta}{2}}_{z^2-\frac{\alpha+\beta}{2},\frac{\alpha-\beta}{2},\frac{-\alpha+\beta}{2},-\frac{\alpha+\beta}{2}}\right). \tag{18}$$

and

$$\beta=\left[\exp\left(\frac{0.51\delta_R^2}{\left(1+0.69\delta_R^{12/5}\right)^{5/6}}\right)-1\right]^{-1}, \tag{15}$$

where $\delta_R^2=1.23C_n^2K_1^{7/6}{d_{U,D}}^{11/6}$ refers to the Rytov variance for plane waves, C_n^2 and K_1 are the refractive index structure parameter and the wave numbers, and $d_{U,D}$ is the distance between the UAV and HAP.

Substituting (11), (12), (13) into (10), the PDF of $h_{U,D}$ can be obtained as

$$\begin{aligned}f_{h_{U,D}}(h)\;=\;&\frac{(\alpha\beta)^{(\alpha+\beta)/2}z^2}{h\Gamma(\alpha)\Gamma(\beta)h_l^{z^2}}\left(\frac{h}{A_0}\right)^{\frac{\alpha+\beta}{2}}\\&\times G_{1,3}^{3,0}\left(\frac{\alpha\beta h}{A_0h_l}\,\middle|\,{}^{1+z^2-\frac{\alpha+\beta}{2}}_{z^2-\frac{\alpha+\beta}{2},\frac{\alpha-\beta}{2},\frac{-\alpha+\beta}{2}}\right),\end{aligned} \tag{16}$$

where $G_{p,q}^{m,n}(\cdot)$ is the Meijer's G-function. Therefore, the PDF and CDF of $\gamma_{U,D}$ obtained in (17) and (18) are shown at the top of this page, respectively. The derivation steps of (17) and (18) are presented in Appendix B.

III. SECURITY PERFORMANCE ANALYSIS

In this section, the end-to-end channel distribution of the legitimate and wiretap links is first studied, followed by the secrecy outage probability analysis. Then we provide the closed-form of asymptotic SOP and PPSC at high SNR regions. Moreover, the diversity order of both the legitimate and the wiretap links is derived.

A. End to End Channel Statistical Characteristics

This section presents the end-to-end statistical characteristics of legitimate and wiretap links under the opportunistic user scheduling (OUS) scheme. The highest SNR among the users is written as

$$\gamma_{\rm sel}=\max_{k=1,\ldots,K}\left\{\gamma_{1,U},\gamma_{2,U},\ldots,\gamma_{K,U}\right\}. \tag{19}$$

The CDF of instantaneous SNR from the scheduled user (S) to U can be obtained as

$$\begin{aligned}F_{\gamma_{S,U}}(\gamma)&=\prod_{k=1}^{K}F_{\gamma_{k,U}}(\gamma)\\&=\prod_{k=1}^{K}\left(1-\sum_{p=0}^{\eta-1}\exp\left(-\lambda_{k,\gamma}\right)\frac{(\lambda_{k,\gamma})^p}{p!}\right)\\&=\sum_{k=0}^{K}\frac{(-1)^k}{k!}\sum_{n_1,\ldots,n_k}^{K}\sum_{q=0}^{\eta-1}\varpi_q\gamma^{\frac{q}{2}}\exp\left(-\lambda_{\rm sum}\gamma^{\frac{1}{2}}\right),\end{aligned} \tag{20}$$

where $\lambda_{k,\gamma}=\frac{\sqrt{\gamma}}{\lambda_k}$, $\lambda_{\rm sum}=\sum_{t=1}^{k}\frac{1}{\lambda_{n_t}}$ and $\varpi_q=\sum_{|o_t|}\frac{1}{\lambda_k^{p_{n_t}}\times p_{n_t}!}$. The operator $|o_t|$ denotes the cardinality of the set o_t which includes all terms having the order of q [33].

With DF protocol, the CDF of the legitimate link from S to D is given by (21) shown at top of the this page, where the term $\hat{M}=\frac{z^2}{\zeta\Gamma(\alpha)\Gamma(\beta)h_l^{z^2}}\left(\frac{\alpha\beta}{A_0\sqrt{\bar{\gamma}_{U,D}}}\right)^{\frac{\alpha+\beta}{2}}$ is a constant.

Lemma 2. *For the wiretap channel between S and E, the PDF and CDF of instantaneous SNR can be written as*

$$f_{\gamma_{S,E}}(\gamma)=\left(\frac{m}{\bar{\gamma}_{S,E}}\right)^m\left(\frac{\gamma^{m-1}}{\Gamma(m)}\right)G_{0,1}^{1,0}\left(\frac{m\gamma}{\bar{\gamma}_{S,E}}\,\middle|\,{}^{-}_{0}\right), \tag{22}$$

and

$$F_{\gamma_{S,E}}(\gamma)=1-\frac{1}{\Gamma(m)}G_{1,2}^{2,0}\left(\frac{m\gamma}{\bar{\gamma}_{S,E}}\,\middle|\,{}^{1}_{m,0}\right). \tag{23}$$

□

Proof. Please see Appendix C. ■ □

B. Secrecy Outage Probability

Aided by the channel characteristics given in subsection A, now we provide the SOP. The instantaneous secrecy rate C_s is defined as the data rate difference between legitimate and wiretap links, written as

$$C_s\left(\gamma_{S,D},\gamma_{S,E}\right)=\left[\ln\left(1+\gamma_{S,D}\right)-\ln\left(1+\gamma_{S,E}\right)\right]^+, \tag{24}$$

where $[x]^+=\max\{x,0\}$. The SOP is defined as the probability that C_s falls below a predetermined secrecy rate threshold

$$F_{\gamma_{S,D}}(\gamma) = \Pr\{\min\{\gamma_{S,U}, \gamma_{U,D}\} < \gamma\} = 1 - \left(1 - F_{\gamma_{S,U}}(\gamma)\right)\left(1 - F_{\gamma_{U,D}}(\gamma)\right)$$
$$= \sum_{k=0}^{K} \frac{(-1)^k}{k!} \sum_{n_1,\ldots,n_k}^{K} \sum_{q=0}^{\eta-1} \varpi_q \gamma^{\frac{q}{2}} \exp\left(-\lambda_{\text{sum}} \gamma^{\frac{1}{2}}\right) + \hat{M} \gamma^{\frac{\alpha+\beta}{4}} G_{2,4}^{3,1}\left(\frac{\alpha\beta\sqrt{\frac{\gamma}{\bar{\gamma}_{U,D}}}}{A_0 h_l}\middle|_{z^2-\frac{\alpha+\beta}{2}, \frac{\alpha-\beta}{2}, \frac{-\alpha+\beta}{2}, -\frac{\alpha+\beta}{2}}^{1-\frac{\alpha+\beta}{2}, 1+z^2-\frac{\alpha+\beta}{2}}\right) \quad (21)$$
$$- \left(\sum_{k=0}^{K} \frac{(-1)^k}{k!} \sum_{n_1,\ldots,n_k}^{K} \sum_{q=0}^{\eta-1} \varpi_q \gamma^{\frac{q}{2}} \exp\left(-\lambda_{\text{sum}} \gamma^{\frac{1}{2}}\right)\right) \hat{M} \gamma^{\frac{\alpha+\beta}{4}} G_{2,4}^{3,1}\left(\frac{\alpha\beta\sqrt{\frac{\gamma}{\bar{\gamma}_{U,D}}}}{A_0 h_l}\middle|_{z^2-\frac{\alpha+\beta}{2}, \frac{\alpha-\beta}{2}, \frac{-\alpha+\beta}{2}, -\frac{\alpha+\beta}{2}}^{1-\frac{\alpha+\beta}{2}, 1+z^2-\frac{\alpha+\beta}{2}}\right)$$

R_s, expressed as

$$P_{\text{out}} = \Pr\{C_s(\gamma_{S,D}, \gamma_{S,E}) \le R_s\}$$
$$= \Pr\{\gamma_{S,D} \le \Theta(\gamma_{S,E} + 1) - 1\}$$
$$= \int_0^{\infty} F_{\gamma_{S,D}}(\Theta(\gamma+1) - 1) f_{\gamma_{S,E}}(\gamma) d\gamma \quad (25)$$
$$\overset{a}{\approx} \int_0^{\infty} F_{\gamma_{S,D}}(\Theta\gamma) f_{\gamma_{S,E}}(\gamma) d\gamma,$$

where $\Theta = 2^{R_s}$. The step "a" for approximation provides a tight lower bound of the SOP with the small R_s or large $\bar{\gamma}_{S,E}$. Substituting (21) and (22) into (25), we derive the SOP as

$$P_{\text{out}} = I_1 + I_2 - I_3, \quad (26)$$

where

$$I_1 = \sum_{k=0}^{K} \frac{(-1)^k}{k!} \sum_{n_1,\ldots,n_k}^{K} \sum_{q=0}^{\eta-1} V H_{1,1}^{1,1} \quad (27)$$
$$\left[\frac{m}{\bar{\gamma}_{S,E}\lambda_\Theta{}^2}\middle| \begin{matrix}(0,1),(1-q-2m,2),(0,1)\\(0,1),(1-q-2m,2),(0,1)\end{matrix}\right],$$

$$I_2 = \hat{M}\hat{V} A_\Theta^{-\frac{\alpha+\beta}{2}-2m} H_{4,3}^{2,3}\left(\frac{m}{\bar{\gamma}_{S,E} A_\Theta^2}\middle| \begin{matrix}(0,1),E_1,(0,1)\\(0,1),E_2,(0,1)\end{matrix}\right), \quad (28)$$

and

$$I_3 = \hat{M} \times \sum_{k=0}^{K} \frac{(-1)^k}{k!} \sum_{n_1,\ldots,n_k}^{K} \sum_{q=0}^{\eta-1} \tilde{V} \lambda_\Theta^{1-q-\frac{\alpha+\beta}{2}-2m} \times \quad (29)$$
$$G_{1,0:2,4:0,1}^{0,1:3,1:1,0}\left(\begin{matrix}1-q-\frac{\alpha+\beta}{2}-2m\\1-q-\frac{\alpha+\beta}{2}-2m\end{matrix}\middle| \begin{matrix}E_3\\E_4\end{matrix}\middle| 0 \middle| \frac{A_\Theta}{\lambda_\Theta}, \frac{m}{\bar{\gamma}_{S,E}\lambda_\Theta}\right).$$

Proof. Please see Appendix D. ■ □

C. Asymptotic Secrecy Outage Probability

In section III-B, we obtained a closed-form expression for SOP in form of Meijer's G-function and Fox's H-function, which however is too complicated to analyze performance. Therefore, to acquire explicit insights, in this section, the asymptotic SOP (i.e., written as $\tilde{P}_{\text{out}}$) is calculated for high SNR regions. Eventually, the diversity order G_d will be conducted by the relation $\tilde{P}_{\text{out}} \approx (G_c SNR)^{-G_d}$, where G_c is the coding gain.

Leveraging $\bar{\gamma}_{S,U} \to \infty$ and the Taylor series of the incomplete gamma function, the CDF of the instantaneous SNR from S to U in (20) is simplified as

$$F_{\gamma_{S,U}}^{\infty}(\gamma) = \prod_{k=1}^{K} \frac{1}{\eta!}\left(\frac{1}{\bar{\lambda}}\right)^{\eta} \gamma^{\frac{\eta}{2}}. \quad (30)$$

Since the users' spacing is much smaller than the distance of users to RIS, channels from S to U are readily deemed as independent and identically distributed ($\lambda_i = \bar{\lambda}$, $d_{i,R} = d_{S,R}, i \in \mathbb{K} = \{1, 2, ..., K\}$). Therefore, the CDF in (30) can be simplified as

$$F_{\gamma_{S,U}}^{\infty}(\gamma) = \left(\frac{1}{\eta!}\right)^{K}\left(\frac{1}{\bar{\lambda}}\right)^{\eta K} \gamma^{\frac{\eta K}{2}}. \quad (31)$$

For the FSO link, as $\bar{\gamma}_{U,D} \to \infty$, the Meijer's G-Function in (18) is derived as the following series representation with higher order terms omitted [34, Eq. (07.34.06.0006.01)]

$$G_{2,4}^{3,1}\left(\frac{\alpha\beta}{A_0 h_l}\sqrt{\frac{\gamma}{\bar{\gamma}_{U,D}}}\middle|_{z^2-\frac{\alpha+\beta}{2}, \frac{\alpha-\beta}{2}, \frac{-\alpha+\beta}{2}, -\frac{\alpha+\beta}{2}}^{1-\frac{\alpha+\beta}{2}, 1+z^2-\frac{\alpha+\beta}{2}}\right)$$
$$= \sum_{i=1}^{3} \frac{\prod_{j=1, j\neq i}^{3} \Gamma(b_j - b_i)\Gamma(1 - a_1 + b_i)}{\Gamma(a_2 - b_i)\Gamma(1 - b_4 + b_i)} (A_{\alpha\beta})^{b_i} \gamma^{\frac{b_i}{2}}, \quad (32)$$

where set $\{a_1, a_2\} = \left\{1 - \frac{\alpha+\beta}{2}, 1 + z^2 - \frac{\alpha+\beta}{2}\right\}$, set $\{b_1, b_2, b_3, b_4\} = \left\{z^2 - \frac{\alpha+\beta}{2}, \frac{\alpha-\beta}{2}, \frac{-\alpha+\beta}{2}, -\frac{\alpha+\beta}{2}\right\}$, and $A_{\alpha\beta} = \frac{\alpha\beta}{A_0 h_l \sqrt{\bar{\gamma}_{U,D}}}$.

Therfore, the CDF in (18) is given as

$$F_{\gamma_{U,D}}^{\infty}(\gamma) = \sum_{i=1}^{3} \frac{\prod_{j=1, j\neq i}^{3} \Gamma(b_j - b_i)\Gamma(1 - a_1 + b_i)}{\Gamma(a_2 - b_i)\Gamma(1 - b_4 + b_i)} \hat{M}$$
$$\times (A_{\alpha\beta})^{b_i} \gamma^{\frac{b_i}{2} + \frac{\alpha+\beta}{4}} \quad (33)$$
$$\approx \Psi \times \gamma^{\frac{v}{2} + \frac{\alpha+\beta}{4}},$$

where $v = \min\{b_1, b_2, b_3, b_4\}$ and Ψ is a constant such that

$$\Psi = \sum_{i=1}^{3} \frac{\prod_{j=1, j\neq i}^{3} \Gamma(b_j - b_i)\Gamma(1 - a_1 + b_i)}{\Gamma(a_2 - b_i)\Gamma(1 - b_4 + b_i)} \hat{M} (A_{\alpha\beta})^{b_i}. \quad (34)$$

In addition, the CDF of $\gamma_{S,D}$ at high SNR becomes

$$F_{\gamma_{S,D}}^{\infty}(\gamma) \approx F_{\gamma_{S,U}}^{\infty}(\gamma) + F_{\gamma_{U,D}}^{\infty}(\gamma)$$
$$\approx \left(\frac{1}{\eta!}\right)^{K}\left(\frac{1}{\bar{\lambda}}\right)^{\eta K} \gamma^{\frac{\eta K}{2}} + \Psi \times \gamma^{\frac{v}{2} + \frac{\alpha+\beta}{4}} \quad (35)$$

Substituting (22) and (35) into (25), the asymptotic SOP is written as

$$\begin{aligned} P_{\text{out}}^{\infty} &= \int_0^{\infty} F_{\gamma_{S,D}}^{\infty}(\Theta\gamma) f_{\gamma_{S,E}}(\gamma)\,\mathrm{d}\gamma \\ &= \int_0^{\infty} \left(\left(\frac{1}{\eta!}\right)^K \left(\frac{1}{\bar{\bar{\lambda}}}\right)^{\eta K} (\Theta\gamma)^{\frac{\eta K}{2}} + \Psi \times (\Theta\gamma)^{\frac{v}{2}+\frac{\alpha+\beta}{4}} \right) \\ &\times \left(\frac{m}{\bar{\gamma}_{S,E}}\right)^m \left(\frac{\gamma^{m-1}}{\Gamma(m)}\right) \exp\left(\frac{-m\gamma}{\bar{\gamma}_{S,E}}\right) \mathrm{d}\gamma \\ &= \tilde{I}_1 + \tilde{I}_2, \end{aligned} \tag{36}$$

where $\tilde{I}_1$ and $\tilde{I}_2$ are written as

$$\begin{aligned} \tilde{I}_1 &= \int_0^{\infty} \left(\frac{1}{\eta!}\right)^K \left(\frac{1}{\bar{\bar{\lambda}}}\right)^{\eta K} (\Theta\gamma)^{\frac{\eta K}{2}} \\ &\times \left(\frac{m}{\bar{\gamma}_{S,E}}\right)^m \left(\frac{\gamma^{m-1}}{\Gamma(m)}\right) \exp\left(\frac{-m\gamma}{\bar{\gamma}_{S,E}}\right) \mathrm{d}\gamma, \end{aligned} \tag{37}$$

$$\begin{aligned} \tilde{I}_2 &= \int_0^{\infty} \Psi \times (\Theta\gamma)^{\frac{v}{2}+\frac{\alpha+\beta}{4}} \\ &\times \left(\frac{m}{\bar{\gamma}_{S,E}}\right)^m \left(\frac{\gamma^{m-1}}{\Gamma(m)}\right) \exp\left(\frac{-m\gamma}{\bar{\gamma}_{S,E}}\right) \mathrm{d}\gamma. \end{aligned} \tag{38}$$

After some simple manipulations, $\tilde{I}_1$ and $\tilde{I}_2$ can be finally expressed as

$$\tilde{I}_1 = B_1 \Gamma\left(\frac{\eta K}{2} + m\right) \bar{\gamma}_{S,U}^{-\frac{\eta K}{2}}, \tag{39}$$

and

$$\tilde{I}_2 = B_2 \Gamma\left(\frac{v}{2} + \frac{\alpha+\beta}{4} + m\right) \bar{\gamma}_{U,D}^{-\frac{v}{2}-\frac{\alpha+\beta}{4}}, \tag{40}$$

where B_1 and B_2 are given as follow

$$B_1 = \left(\frac{1}{\eta!}\right)^K \frac{1}{\Gamma(m)} \left(\frac{4\pi d_{S,R} d_{R,U}}{16-\pi^2}\right)^{\eta K} \left(\frac{\Theta\bar{\gamma}_{S,E}}{m}\right)^{\frac{\eta K}{2}}, \tag{41}$$

and

$$\begin{aligned} B_2 &= \frac{z^2}{\zeta \Gamma(\alpha)\Gamma(\beta) h_l^{z^2}} \left(\frac{\alpha\beta}{A_0}\right)^{\frac{\alpha+\beta}{2}} \frac{1}{\Gamma(m)} \left(\frac{\Theta\bar{\gamma}_{S,E}}{m}\right)^{\frac{v}{2}+\frac{\alpha+\beta}{4}} \\ &\times \sum_{i=1}^{3} \frac{\prod_{j=1, j\neq i}^{3} \Gamma(b_j - b_i)\,\Gamma(1-a_1+b_i)}{\Gamma(a_2-b_i)\,\Gamma(1-b_4+b_i)} \left(\frac{\alpha\beta}{A_0 h_l}\right)^{b_i}. \end{aligned} \tag{42}$$

Finally, substituting (39) and (40) into (36), the asymptotic SOP is derived[3]. Therefore, the diversity order is given as

$$G_d = \min\left\{\frac{\eta K}{2}, \frac{v}{2} + \frac{\alpha+\beta}{4} - 1\right\}. \tag{43}$$

Remark 1. *The result shows that the secrecy performance for the RIS-based mixed FSO/RF two-layer heterogeneous networks is dominated by the weaker one between the RF and the FSO channel links. In the RF dominating case (i.e., $G_d = \frac{\eta K}{2}$), the system performance is dependent on the shape parameter η and the number of users K, then the coding gain becomes*

$$G_c = \left(B_1 \Gamma\left(\frac{\eta K}{2} + m\right)\right)^{\frac{\eta K}{2}}, \tag{44}$$

while in the FSO link dominating case (i.e., $G_d = \frac{v}{2} + \frac{\alpha+\beta}{4} - 1$), the system performance is dependent on the parameter of PE, i.e., the value of z^2, the large-scale and small-scale scattering parameter α and β, and then the coding gain is

$$G_c = \left(B_2 \Gamma\left(\frac{v}{2} + \frac{\alpha+\beta}{4} + m\right)\right)^{\frac{v}{2}+\frac{\alpha+\beta}{4}}. \tag{45}$$

D. Asymptotic Probability of Positive Secrecy Capacity

The PPSC is another secrecy performance metric based on Wyner's model, defined as the probability that C_s is positive and expressed as

$$\begin{aligned} P_{\text{ppsc}} &= \Pr[C_s > 0] = \Pr[\gamma_{S,D} > \gamma_{S,E}] \\ &= 1 - \int_0^{\infty} F_{\gamma_{S,D}}(\gamma) f_{\gamma_{S,E}}(\gamma) \mathrm{d}\gamma. \end{aligned} \tag{46}$$

At high SNRs, the asymptotic PPSC can be obtained by substituting(22) and (35) into (46) such that

$$\begin{aligned} P_{\text{ppsc}} &= 1 - \int_0^{\infty} \left(\left(\frac{1}{\eta!}\right)^K \left(\frac{1}{\bar{\bar{\lambda}}}\right)^{\eta K} \gamma^{\frac{\eta K}{2}} + \Psi \times \gamma^{\frac{v}{2}+\frac{\alpha+\beta}{4}} \right) \\ &\times \left(\frac{m}{\bar{\gamma}_{S,E}}\right)^m \left(\frac{\gamma^{m-1}}{\Gamma(m)}\right) \exp\left(\frac{-m\gamma}{\bar{\gamma}_{S,E}}\right) \mathrm{d}\gamma \\ &= 1 - \tilde{B}_1 \left(\frac{\bar{\gamma}_{S,E}}{m}\right)^{\frac{\eta K}{2}} \Gamma\left(\frac{\eta K}{2} + m\right) \\ &- \tilde{B}_2 \left(\frac{\bar{\gamma}_{S,E}}{m}\right)^{\frac{v}{2}+\frac{\alpha+\beta}{4}} \Gamma\left(\frac{v}{2} + \frac{\alpha+\beta}{4} + m\right), \end{aligned} \tag{47}$$

where the expressions of $\tilde{B}_1$ and $\tilde{B}_2$ are

$$\tilde{B}_1 = \left(\frac{1}{\eta!}\right)^K \left(\frac{1}{\bar{\bar{\lambda}}}\right)^{\eta K} \frac{1}{\Gamma(m)}, \tag{48}$$

and

$$\tilde{B}_2 = \frac{\Psi}{\Gamma(m)}. \tag{49}$$

The exponential term in (47) contains the number of users K, RIS elements N, and the factor of FSO fading parameters, such as α, β, z. These parameters play a crucial role in the secrecy performance of the system and we will show their impact in the next section.

IV. Simulation Results

In this section, the numerical results of the derived secure analysis are shown. The CDF of end-to-end SNR for legitimate and wiretap links is first demonstrated. Subsequently, the SOPs under various parameters (such as K, N, α, etc.) are compared

[3]The expression includes 71 additions, $K(N-1)+67$ multiplications, and 24 Gamma functions, whose exponential term is $\left\{\frac{3}{2}NK, \frac{v}{2} + \frac{3}{4}(\alpha+\beta)\right\}$

and the asymptotic SOPs at the high SNR regions are also illustrated[4]. In addition, we compare the OUS scheme with the round-robin user scheduling (RrUS) [37] scheme in the presence and absence of RIS to verify the superiority of this framework. Finally, the analytical expressions for the asymptotic PPSC are also compared under different parameter cases. The main simulation parameters are shown in Table I[5]

TABLE I
SIMULATION PARAMETERS

Parameter	Value
Number of RIS elements, N	10∼20
Number of ground users, K	2∼4
Fading parameter, m	2∼3
Pass loss of FSO channel, h_l	0.741
Constant term of PE, A_0	0.8
Electrical-optical conversion coefficient, ζ	0.5
Moderate Turbulence $[\alpha, \beta]$	[5.42,3.8]
Strong Turbulence $[\alpha, \beta]$	[4,1.71]
Secure transmission threshold, R_s	0.01 bps
Distance from the UAV to HAP, $d_{U,D}$	800 m

Figure 2 shows the CDFs of the instantaneous SNR of the mixed RF/FSO networks from users to UAV, users to Eve, and UAV to HAP, respectively. Comparisons are also performed under strong and weak atmospheric turbulence, different numbers of RIS elements, and different fading factors, while MC simulations demonstrate the accuracy of our analysis results. It can be seen that all six curves converge to 1 when the SNR is 25 dB, hence we treat $\gamma = 25$ dB as $\gamma \to \infty, \gamma \in \{\gamma_{S,U}, \gamma_{U,D}\}$ in the following simulations of the asymptotic SOP and PPSC.

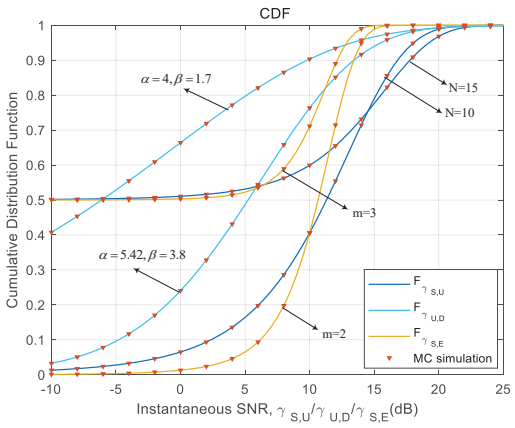

Fig. 2. CDFs of instantaneous SNR for the mixed RF/FSO networks

Figure 3 shows the variations of SOP with the number of users for strong and moderate turbulence conditions, respectively, where the transmission SNR means $\bar{\gamma}_{S,U}$ or $\bar{\gamma}_{U,D}$ cause we equalize these two parameters at simulation. It can be seen that the SOP decreases as the number of users increases, which implies that the SOP in a single-user scenario is an upper bound for that in a multi-user one, and this conclusion can provide vital insight for future works. Moreover, the derived analytical results are identical to the MC simulations and gradually approximate the asymptotic SOP curve when the transmission SNR is high enough, both of which validate the accuracy of the performance metrics for the proposed system.

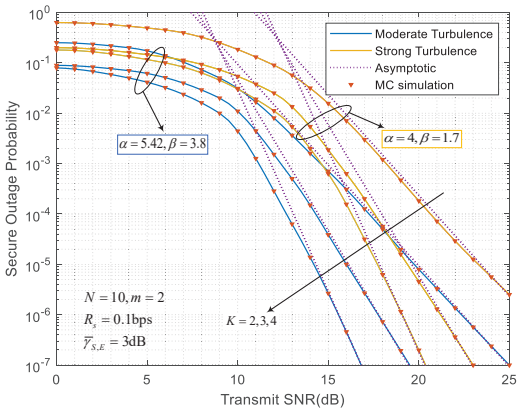

Fig. 3. SOP for varying K under different atmospheric turbulence conditions with the asymptotic results at high SNR regions.

Figure 4 shows the variations of SOP with the number of RIS elements for strong and moderate turbulence conditions, respectively. It is obvious that larger N can achieve lower SOP, and their curve slope is also larger. The blue curve in the figure indicates moderate turbulence ($\alpha = 5.42$ and $\beta = 3.8$), where the SOP is about 2% for RIS element number $N = 20$ and about 10% for $N = 10$ at a low transmission SNR of 0 dB, a difference of 5 times. This indicates that we can improve the safety performance of mixed RF/FSO systems effectively by increasing the number of RIS components. Similar to Fig. 3, the MC simulations and the asymptotic expressions at high SNR can confirm the correctness of our derivation.

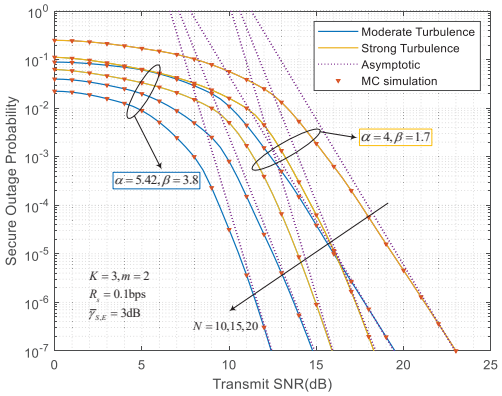

Fig. 4. SOP for varying N under different atmospheric turbulence conditions with the asymptotic results at high SNR regions.

Figure 5 shows the variations of SOP with $\bar{\gamma}_{S,E}$ for strong and moderate turbulence conditions with $N = 15, K = 3$,

[4]The numerical evaluation for Fox's H-function and bivariate Meijer's G-functions are based on [35, APPENDIX A] and [36, TABLE II].

[5]The altitude of HAP is set to 1 km. The frequency and bandwidth for the RF channel are 2.1 GHz and 20 MHz, respectively [38].

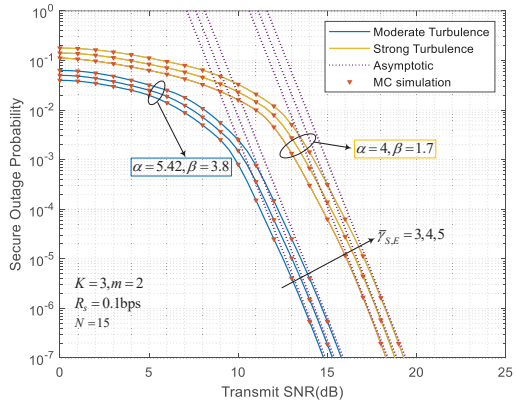

Fig. 5. SOP for varying $\bar{\gamma}_{S,E}$ under different atmospheric turbulence conditions with the asymptotic results at high SNR regions.

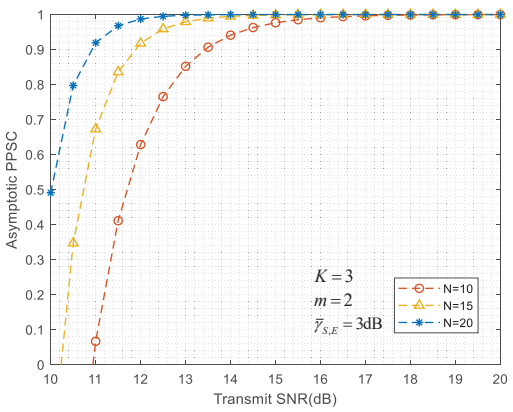

Fig. 7. Asymptotic PPSC varying N under moderate atmospheric turbulence conditions at high SNR regions.

respectively. The SOP decreases as the wiretap SNR $\bar{\gamma}_{S,E}$ decreases and approaches the asymptotic curve at high SNR. It is worth noting that the slopes of the six asymptotic curves are the same because in (39) and (40), $\bar{\gamma}_{S,E}$ is the product term factor of the transmission SNR ($\bar{\gamma}_{S,U}$ or $\bar{\gamma}_{U,D}$) while K, N, α and β are the exponential term factors, with the latter being significantly more influential than the former. Therefore, it can be concluded that our proposed framework can effectively improve the security performance of the system, regardless of the quality of the wiretap link.

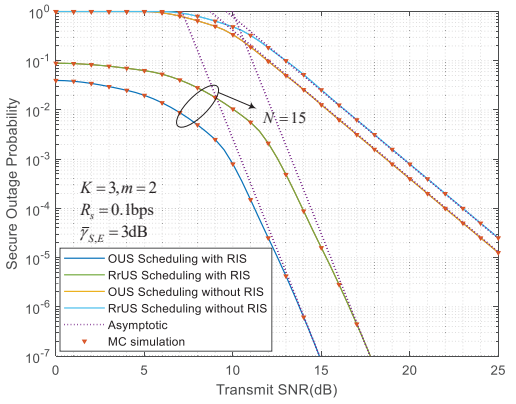

Fig. 6. SOP for OUS vs. RrUS scheduling scheme in the presence or absence of RIS with the asymptotic results at high SNR regions.

Figure 6 compares our proposed OUS scheduling scheme with RrUS scheme in the presence and absence of RIS. In the RrUS scheme, each user has the same probability to transmit rather than the optimal user. It can be seen that our scheme has a superior performance advantage over the RrUS scheme, while the SOP of the system is much lower when RIS components $N = 15$ than that is absent. To be more specific, the OUS scheme improves the system secrecy performance (about 10^{-7}) by 100 times over the RrUS scheme (about 10^{-5}) at high transmission SNR in the presence of RIS, both of which prove the effectiveness of our proposed framework.

Figure 7 shows the trend of Asymptotic PPSC with transmission SNR for various N. It can be observed that the asymptotic PPSC at variable elements N of RIS converges to 1 as the transmission SNR is more than 15. Moreover, perfectly positive secrecy capacity can be achieved with smaller signal-to-noise ratios when N is gradually increased, e.g. N = 20, which further confirms that the introduction of RIS can effectively improve the security metrics of this mixed RF/FSO system.

Figure 8 shows the asymptotic PPSC varying simultaneously with $\bar{\gamma}_{S,U}$ and $\bar{\gamma}_{S,E}$, where $K = 3$, $N = 10$, $\alpha = 4$, and $\beta = 1.71$. In the event of strong turbulence, any smaller eavesdropping SNR e.g.$\bar{\gamma}_{S,E} = 4$ dB, may lead to a non-positive secrecy capacity, which implies that measures increasing the gap between the channel state of the legitimate link and the wiretap link required to be implemented, such as increasing the number of RIS elements or using superior scheduling methods.

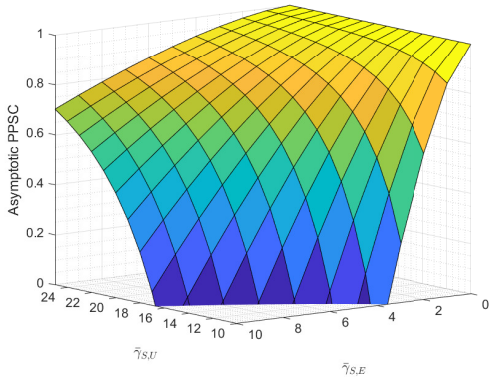

Fig. 8. Asymptotic PPSC versus $\bar{\gamma}_{S,U}$ and $\bar{\gamma}_{S,E}$ under strong atmospheric turbulence conditions at high SNR regions.

V. Conclusion

A novel RIS-assisted HAP-UAV collaborative multi-user mixed RF/FSO system was proposed in this paper. First, we derived the end-to-end channel statistical characteristics for both legitimate and wiretap links, where the effects of pointing errors, path loss, and atmospheric turbulence were taken into

account capturing the propagation characteristics of the FSO link. Second, a closed-form solution for SOP is derived from the perspective of Meijer's G-function. Moreover, the diversity order and coding gain for the mixed RF/FSO system were achieved to acquire more explicit insights, and the asymptotic PPSC expression was derived at high SNR regions. Finally, the simulation verifies the correctness of the derived results, as well as the tightness of the asymptotic expressions.

APPENDIX A

First, we introduce the symbol $\mathcal{B} = \sqrt{\gamma_{k,U}} = \sqrt{\bar{\gamma}_{S,U}}\left(\sum_{n=1}^{N} x_n y_n\right)$ to simplify the derivation, where $x_n = \left|h_{R,U}^{k,n}\right|$ and $y_n = \left|h_{S,R}^{k,n}\right|$ are the Rayleigh RVs. The derivation of the CDF of $\mathcal{B}$ involves multiplying and adding various RVs, making it challenging. To simplify the process, a moment-matching method that utilizes a regular Gamma distribution is employed to approximate $f_{\gamma_{k,U}}$. This technique is widely used to approximate complex distributions [39].

The Gamma RV $\mathcal{B}$ takes shape parameter η and scale parameter λ_k, whose mean and variance are $\mathbb{E}[\mathcal{B}] = \eta\lambda_k$ and $\mathbb{D}[\mathcal{B}] = \eta{\lambda_k}^2$, respectively. Since x_n and y_n are independent Rayleigh RVs, we have $\mathbb{E}[x_n] = \frac{\sqrt{\pi}}{2d_{R,U}}$, $\mathbb{E}\left[x_n^2\right] = d_{R,U}^{-2}$, and similarly $\mathbb{E}[y_n] = \frac{\sqrt{\pi}}{2d_{k,R}}$, $\mathbb{E}\left[y_n^2\right] = d_{k,R}^{-2}$. Therefore, the mean and variance of $\mathcal{B}$ are written as:

$$\mathbb{E}[\mathcal{B}] = N\sqrt{\bar{\gamma}_{S,U}}\mathbb{E}[x_n]\cdot\mathbb{E}[y_n] = \frac{\pi N\sqrt{\bar{\gamma}_{S,U}}}{4d_{R,U}d_{k,R}}, \tag{A.1}$$

and

$$\begin{aligned}\mathbb{D}[\mathcal{B}] &= N\bar{\gamma}_{S,U}\cdot\left[\mathbb{E}[x_n^2]\cdot\mathbb{E}[y_n^2] - \left(\mathbb{E}[x_n]\cdot\mathbb{E}[y_n]\right)^2\right] \\ &= N\bar{\gamma}_{S,U}\cdot\tfrac{16-\pi^2}{16d_{R,U}^2 d_{k,R}^2}.\end{aligned} \tag{A.2}$$

Therefore, the shape parameter η and scale parameter λ_k can be obtained as

$$\eta = \frac{D[\mathcal{B}]}{E[\mathcal{B}]} = \frac{\sqrt{\bar{\gamma}_{S,U}}\left(16-\pi^2\right)}{4\pi d_{R,U}d_{k,R}}, \tag{A.3}$$

and

$$\lambda_k = \frac{E[\mathcal{B}]}{\eta} = \frac{N\pi^2}{16-\pi^2}. \tag{A.4}$$

Finally, after substituting the above equations into the Gamma distribution, the statistic function in Lemma 1 can be obtained with RV $\gamma_{k,U} = \mathcal{B}^2$.

APPENDIX B

A. Steps in the derivation of (13)

Since h_p and h_t are two independent random variables, while h_l is a constant related only to distance, the PDF of $h_{U,D}$ can be derived from

$$\begin{aligned}f_{h_{U,D}}(h) =& \frac{1}{h_l}\int_{h/h_l A_0}^{\infty}\frac{1}{x}f_{h_t}(x)\,f_{h_p}\left(\frac{h}{xh_l}\right)\mathrm{d}x \\ =& \frac{1}{h_l}\int_{h/h_l A_0}^{\infty}\frac{1}{x}\frac{2(\alpha\beta)^{(\alpha+\beta)/2}}{\Gamma(\alpha)\Gamma(\beta)}x^{\frac{\alpha+\beta}{2}-1} \\ &\times K_{\alpha-\beta}\left(2\sqrt{\alpha\beta x}\right)\frac{z^2}{A_0^{z^2}}\left(\frac{h}{h_l x}\right)^{z^2-1}\mathrm{d}x.\end{aligned} \tag{B.1}$$

After the variable substitution $\mu = \frac{h_l A_0}{h}x$ and with the help of [40, Eq. (09.34.3)], the above equtaion can be further written as

$$f_{h_{U,D}}(h) = M\int_1^{\infty}\mu^{\frac{\alpha+\beta}{2}-1-z^2}G_{0,2}^{2,0}\left(\frac{\alpha\beta h\mu}{A_0 h_l}\middle|\frac{\alpha-\beta}{2},\frac{-\alpha+\beta}{2}\right)\mathrm{d}\mu, \tag{B.2}$$

where M is the constant part independent of h and expressed as

$$M = \frac{(\alpha\beta)^{(\alpha+\beta)/2}z^2}{h\Gamma(\alpha)\Gamma(\beta)h_l^{z^2}}\left(\frac{h}{A_0}\right)^{\frac{\alpha+\beta}{2}}. \tag{B.3}$$

According to [40, Eq. (07.811.3)], the final PDF of $h_{U,D}$ can be obtained as

$$\begin{aligned}f_{h_{U,D}}(h) &= \frac{(\alpha\beta)^{(\alpha+\beta)/2}z^2}{h\Gamma(\alpha)\Gamma(\beta)h_l^{z^2}}\left(\frac{h}{A_0}\right)^{\frac{\alpha+\beta}{2}} \\ &\times G_{1,3}^{3,0}\left(\frac{\alpha\beta h}{A_0 h_l}\middle|\begin{matrix}1+z^2-\frac{\alpha+\beta}{2}\\ z^2-\frac{\alpha+\beta}{2},\frac{\alpha-\beta}{2},\frac{-\alpha+\beta}{2}\end{matrix}\right).\end{aligned} \tag{B.4}$$

B. Steps in the derivation of (17) and (18)

By using $h_{U,D} = \frac{1}{\zeta}\sqrt{\frac{\gamma_{U,D}}{\bar{\gamma}_{U,D}}}$ and substituting it into Eqs. (B.5), Eqs. (17) can be derived after some mathematical operations related to the distribution of functions of random variables. Afterwards, the CDF of $\gamma_{U,D}$ can be obtained by means of integrating Eqs. (17) as

$$\begin{aligned}F_{\gamma_{U,D}}(\gamma) &= \int_0^{\gamma}f_{\gamma_{U,D}}(x)\mathrm{d}x \overset{(a)}{=} \tilde{M}\int_0^1 y^{\frac{\alpha+\beta}{2}-1} \\ &\times G_{1,3}^{3,0}\left(\frac{\alpha\beta}{A_0 h_l}\sqrt{\frac{\gamma}{\bar{\gamma}_{U,D}}}y\middle|\begin{matrix}1+z^2-\frac{\alpha+\beta}{2}\\ z^2-\frac{\alpha+\beta}{2},\frac{\alpha-\beta}{2},\frac{-\alpha+\beta}{2}\end{matrix}\right)\mathrm{d}y,\end{aligned} \tag{B.5}$$

where (a) is the variable substitutions $x = \gamma\times y^2$ and $\tilde{M}$ is the constant part independent of variable of integration y and expressed as

$$\tilde{M} = \frac{z^2}{\zeta\Gamma(\alpha)\Gamma(\beta)h_l^{z^2}}\left(\frac{\alpha\beta\sqrt{\gamma}}{A_0\sqrt{\bar{\gamma}_{U,D}}}\right)^{\frac{\alpha+\beta}{2}}. \tag{B.6}$$

Moreover, after some algebraic operations [40, Eq. (07.811.2)], the Eq. (18) can be obtained.

APPENDIX C

It is assumed that the channels from the users to the UAV are i.i.d. RVs, hence we have

$$\begin{aligned}\Pr\left\{S_k = S_{\text{sel}}\right\} &= \Pr\left\{\max_{\substack{1\le j\le K\\ j\neq k}} \gamma_{j,U} < \gamma_{k,U}\right\}\\ &= \int_0^\infty \prod_{\substack{1\le j\le K\\ j\neq k}} F_{\gamma_{j,U}}(x) f_{k,U}(x)\,\mathrm{d}x\\ &= \int_0^\infty \prod_{\substack{1\le j\le K\\ j\neq k}} F_{\gamma_{j,U}}(x)\mathrm{d}F_{k,U}(x)^{\,6} \quad \text{(C.1)}\\ &= \int_0^\infty \prod_{\substack{1\le j\le K\\ j\neq k}} F_{\gamma_{j,U}}(x)\mathrm{d}F_{j,U}(x)\\ &= \frac{1}{K}{F^K}_{\gamma_{j,U}}(x)\Big|_{0}^{\infty} = \frac{1}{K}.\end{aligned}$$

Therefore the CDF of wiretap channel $F_{\gamma_{S,E}}(\gamma)$ based on the OUS can be expressed as

$$\begin{aligned}F_{\gamma_{S,E}}(\gamma) &= \sum_{k=1}^{K}\Pr\left\{S_k = S_{\text{sel}}\right\}\times F_{\gamma_{k,E}}(\gamma)\\ &= 1-\frac{1}{\Gamma(m)}\Gamma\left(m,\frac{m\gamma}{\bar{\gamma}_{S,E}}\right)\\ &= 1-\frac{1}{\Gamma(m)}G_{1,2}^{2,0}\left(\frac{m\gamma}{\bar{\gamma}_{S,E}}\,\middle|\,\begin{matrix}1\\ m,0\end{matrix}\right), \quad \text{(C.2)}\end{aligned}$$

and the PDF in (22) can be differentiated by (C.2).

APPENDIX D

A. The derivation of I_1

First of all, I_1 is an integral with respect to γ and expressed as

$$\begin{aligned}I_1 = &\int_0^\infty \sum_{k=0}^{K}\frac{(-1)^k}{k!}\sum_{n_1,\ldots,n_k}^{K}\sum_{q=0}^{\eta-1}\varpi_q\times(\Theta\gamma)^{\frac{q}{2}}\exp\left(-\lambda_{\text{sum}}(\Theta\gamma)^{\frac{1}{2}}\right)\\ &\times\frac{\left(\frac{m}{\bar{\gamma}_{S,E}}\right)^m\gamma^{m-1}}{\Gamma(m)}G_{0,1}^{1,0}\left(\frac{m\gamma}{\bar{\gamma}_{S,E}}\,\middle|\,\begin{matrix}-\\ 0\end{matrix}\right)\mathrm{d}\gamma. \quad \text{(D.1)}\end{aligned}$$

Besides, to get rid of the square root term and facilitate the consequent calculation, the substitution $\gamma = t^2$ is introduced. Moreover, with the utilization of [34, Eq. (07.34.03.0004.01)], the above equation is transformed to

$$\begin{aligned}I_1 = &\int_0^\infty \sum_{k=0}^{K}\frac{(-1)^k}{k!}\sum_{n_1,\ldots,n_k}^{K}\sum_{q=0}^{\eta-1}\frac{\varpi_q}{\Gamma(m)}\Theta^{\frac{q}{2}}\left(\frac{m}{\bar{\gamma}_{S,E}}\right)^m\\ &\times t^{q+2m-1}G_{0,1}^{1,0}\left(\frac{mt^2}{\bar{\gamma}_{S,E}}\,\middle|\,\begin{matrix}-\\ 0\end{matrix}\right)G_{0,1}^{1,0}\left(\lambda_\Theta t\,\middle|\,\begin{matrix}-\\ 0\end{matrix}\right)\mathrm{d}t, \quad \text{(D.2)}\end{aligned}$$

where $\lambda_\Theta = \lambda_{\text{sum}}\Theta^{\frac{1}{2}}$.

Furthermore, the Eq. (D.2) can be solved with the assistance of [34, Eq. (07.34.21.0012.01)] and represented as

$$\begin{aligned}I_1 = &\sum_{k=0}^{K}\frac{(-1)^k}{k!}\sum_{n_1,\ldots,n_k}^{K}\sum_{q=0}^{\eta-1}V\times\\ &H_{1,1}^{1,1}\left[\frac{m}{\bar{\gamma}_{S,E}\lambda_\Theta{}^2}\,\middle|\,\begin{matrix}(0,1),(1-q-2m,2),(0,1)\\ (0,1),(1-q-2m,2),(0,1)\end{matrix}\right], \quad \text{(D.3)}\end{aligned}$$

where $V = 2\frac{\varpi_q}{\Gamma(m)}\Theta^{\frac{q}{2}}\left(\frac{m}{\bar{\gamma}_{S,E}}\right)^m$ and $H_{p,q}^{m,n}(\cdot)$ is the Fox's H-function. Therefore, I_1 has been solved completely.

B. The derivation of I_2

The expression I_2 is first written as

$$\begin{aligned}I_2 = &\int_0^\infty G_{2,4}^{3,1}\left(\frac{\alpha\beta\sqrt{\frac{\Theta\gamma}{\bar{\gamma}_{U,D}}}}{A_0h_l}\,\middle|\,\begin{matrix}1-\frac{\alpha+\beta}{2},1+z^2-\frac{\alpha+\beta}{2}\\ z^2-\frac{\alpha+\beta}{2},\frac{\alpha-\beta}{2},\frac{-\alpha+\beta}{2},-\frac{\alpha+\beta}{2}\end{matrix}\right)\\ &\times\hat{M}(\Theta\gamma)^{\frac{\alpha+\beta}{4}}\left(\frac{m}{\bar{\gamma}_{S,E}}\right)^m\frac{\gamma^{m-1}}{\Gamma(m)}G_{0,1}^{1,0}\left(\frac{m\gamma}{\bar{\gamma}_{S,E}}\,\middle|\,\begin{matrix}-\\ 0\end{matrix}\right)d\gamma. \quad \text{(D.4)}\end{aligned}$$

Similar to I_1, with the employment of substitution $\gamma = t^2$ and [34, Eq. (07.34.21.0012.01)], I_2 can be further derived as

$$\begin{aligned}I_2 = &\int_0^\infty \hat{M}\hat{N}\times t^{\frac{\alpha+\beta}{2}+2m-1}\times G_{0,1}^{1,0}\left(\frac{mt^2}{\bar{\gamma}_{S,E}}\,\middle|\,\begin{matrix}-\\ 0\end{matrix}\right)\times\\ &G_{2,4}^{3,1}\left(A_\Theta t\,\middle|\,\begin{matrix}1-\frac{\alpha+\beta}{2},1+z^2-\frac{\alpha+\beta}{2}\\ z^2-\frac{\alpha+\beta}{2},\frac{\alpha-\beta}{2},\frac{-\alpha+\beta}{2},-\frac{\alpha+\beta}{2}\end{matrix}\right)\mathrm{d}t \quad \text{(D.5)}\\ = &\hat{M}\hat{V}A_\Theta^{-\frac{\alpha+\beta}{2}-2m}H_{4,3}^{2,3}\left(\frac{m}{\bar{\gamma}_{S,E}A_\Theta^2}\,\middle|\,\begin{matrix}(0,1),E_1,(0,1)\\ (0,1),E_2,(0,1)\end{matrix}\right),\end{aligned}$$

where $\hat{V} = 2\frac{\Theta^{\frac{\alpha+\beta}{4}}}{\Gamma(m)}\left(\frac{m}{\bar{\gamma}_{S,E}}\right)^m$, $A_\Theta = \frac{\alpha\beta\sqrt{\Theta}}{A_0h_l\sqrt{\bar{\gamma}_{U,D}}}$, $E_1 = \{(1-2m-z^2,2),(1-\alpha-2m,2),(1-\beta-2m,2),(1-2m,2)\}$ and $E_2 = (-2m,2),(-2m-z^2,2)$.

C. The derivation of I_3

The expression of I_3 is

$$\begin{aligned}I_3 = &\sum_{k=0}^{K}\frac{(-1)^k}{k!}\sum_{n_1,\ldots,n_k}^{K}\sum_{q=0}^{\eta-1}\varpi_q\hat{M}\times\int_0^\infty(\Theta\gamma)^{\frac{q}{2}+\frac{\alpha+\beta}{4}}\exp\left(-\lambda_\Theta\gamma^{\frac{1}{2}}\right)\\ &\times G_{2,4}^{3,1}\left(A_\Theta\sqrt{\gamma}\,\middle|\,\begin{matrix}1-\frac{\alpha+\beta}{2},1+z^2-\frac{\alpha+\beta}{2}\\ z^2-\frac{\alpha+\beta}{2},\frac{\alpha-\beta}{2},\frac{-\alpha+\beta}{2},-\frac{\alpha+\beta}{2}\end{matrix}\right) \quad \text{(D.6)}\\ &\times\left(\frac{m}{\bar{\gamma}_{S,E}}\right)^m\frac{\gamma^{m-1}}{\Gamma(m)}G_{0,1}^{1,0}\left(\frac{m\gamma}{\bar{\gamma}_{S,E}}\,\middle|\,\begin{matrix}-\\ 0\end{matrix}\right)\mathrm{d}\gamma.\end{aligned}$$

Utilizing [34, Eq. (07.34.21.0012.01)] with the substitution

$\gamma = t^2$, I_3 becomes

$$I_3 = \hat{M} \times \sum_{k=0}^{K} \frac{(-1)^k}{k!} \sum_{n_1,\ldots,n_k}^{K} \sum_{q=0}^{\eta-1} \tilde{V} \times \int_0^{\infty} t^{q+\frac{\alpha+\beta}{2}+2m-1} G_{0,1}^{1,0}\left(\lambda_\Theta t \,\middle|\, \begin{matrix} - \\ 0 \end{matrix}\right) G_{0,1}^{1,0}\left(\frac{mt^2}{\bar{\gamma}_{S,E}} \,\middle|\, \begin{matrix} - \\ 0 \end{matrix}\right) \times G_{2,4}^{3,1}\left(A_\Theta t \,\middle|\, \begin{matrix} 1-\frac{\alpha+\beta}{2}, 1+z^2-\frac{\alpha+\beta}{2} \\ z^2-\frac{\alpha+\beta}{2}, \frac{\alpha-\beta}{2}, \frac{-\alpha+\beta}{2}, -\frac{\alpha+\beta}{2} \end{matrix}\right) \mathrm{d}t \tag{D.7}$$

$$= \hat{M} \times \sum_{k=0}^{K} \frac{(-1)^k}{k!} \sum_{n_1,\ldots,n_k}^{K} \sum_{q=0}^{\eta-1} \tilde{V} \lambda_\Theta^{1-q-\frac{\alpha+\beta}{2}-2m} \times G_{1,0:2,4:0,1}^{0,1:3,1:1,0}\left(\begin{matrix} 1-q-\frac{\alpha+\beta}{2}-2m \\ 1-q-\frac{\alpha+\beta}{2}-2m \end{matrix} \,\middle|\, \begin{matrix} E_3 \\ E_4 \end{matrix} \,\middle|\, 0 \,\middle|\, \frac{A_\Theta}{\lambda_\Theta}, \frac{m}{\bar{\gamma}_{S,E}\lambda_\Theta}\right),$$

where $\tilde{V} = 2\frac{\varpi_q}{\Gamma(m)}\left(\frac{m}{\bar{\gamma}_{S,E}}\right)^m \Theta^{\frac{q}{2}+\frac{\alpha+\beta}{4}}$, $E_3 = 1-\frac{\alpha+\beta}{2}, 1+z^2-\frac{\alpha+\beta}{2}$ and $E_4 = z^2-\frac{\alpha+\beta}{2}, \frac{\alpha-\beta}{2}, \frac{-\alpha+\beta}{2}, -\frac{\alpha+\beta}{2}$.

Finally, substituting (D.3), (D.5) and (D.7) into (26), the SOP of this system can be obtained.

REFERENCES

[1] C. Chen, Z. Liao, Y. Ju, C. He, K. Yu, and S. Wan, "Hierarchical domain-based multicontroller deployment strategy in SDN-enabled space–air–ground integrated network," *IEEE Trans. Aerosp. Electron. Syst.*, vol. 58, no. 6, pp. 4864–4879, 2022.

[2] L. Yang, Y. Li, S. X. Yang, Y. Lu, T. Guo, and K. Yu, "Generative adversarial learning for intelligent trust management in 6G wireless networks," *IEEE Network*, vol. 36, no. 4, pp. 134–140, 2022.

[3] Y. He, L. Nie, T. Guo, K. Kaur, M. M. Hassan, and K. Yu, "A NOMA-enabled framework for relay deployment and network optimization in double-layer airborne ieee VANETs," *IEEE Trans. Intell. Transp. Syst.*, Feb. 2022.

[4] L. Yang, H. Yao, J. Wang, C. Jiang, A. Benslimane, and Y. Liu, "Multi-UAV-enabled load-balance mobile-edge computing for IoT networks," *IEEE Internet Things J.*, vol. 7, no. 8, pp. 6898–6908, Feb. 2020.

[5] A. Bhowal and R. S. Kshetrimayum, "Outage probability bound of decode and forward two-way relay employing optical spatial modulation over gamma-gamma channels," *IET Optoelectron*, vol. 13, no. 4, pp. 183–190, Aug. 2019.

[6] G. Xu and Q. Zhang, "Mixed RF/FSO deep space communication system under solar scintillation effect," *IEEE Trans. Aerosp. Electron. Syst.*, vol. 57, no. 5, pp. 3237–3251, Apr. 2021.

[7] D. Wang, F. Zhou, W. Lin, Z. Ding, and N. Al-Dhahir, "Cooperative hybrid nonorthogonal multiple ieee-based mobile-edge computing in cognitive radio networks," *IEEE Trans. Cognit. Commun. Networking*, vol. 8, no. 2, pp. 1104–1117, June. 2022.

[8] Y. Wang, Y. Tong, and Z. Zhan, "On secrecy performance of mixed RF-FSO systems with a wireless-powered friendly jammer," *IEEE Photonics J.*, vol. 14, no. 2, pp. 1–8, 2022.

[9] Z. Wei, F. Liu, C. Masouros, and H. V. Poor, "Fundamentals of physical layer anonymous communications: Sender detection and anonymous precoding," *IEEE Trans. Wireless Commun.*, vol. 21, no. 1, pp. 64–79, 2021.

[10] L. Yang, W. Guo, and I. S. Ansari, "Mixed dual-hop FSO-RF communication systems through reconfigurable intelligent surface," *IEEE Commun. Lett.*, vol. 24, no. 7, pp. 1558–1562, 2020.

[11] A. R. Ndjiongue, T. M. Ngatched, O. A. Dobre, A. G. Armada, and H. Haas, "Analysis of RIS-based terrestrial-FSO link over GG turbulence with distance and jitter ratios," *J. Lightwave Technol.*, vol. 39, no. 21, pp. 6746–6758, 2021.

[12] H. Kong, M. Lin, W.-P. Zhu, H. Amindavar, and M.-S. Alouini, "Multiuser scheduling for asymmetric FSO/RF links in satellite-UAV-terrestrial networks," *IEEE Wireless Commun. Lett.*, vol. 9, no. 8, pp. 1235–1239, Aug. 2020.

[13] L. Qu, G. Xu, Z. Zeng, N. Zhang, and Q. Zhang, "UAV-assisted RF/FSO relay system for space-air-ground integrated network: A performance analysis," *IEEE Trans. Wireless Commun.*, vol. 21, no. 8, pp. 6211–6225, Aug. 2022.

[14] G. N. Kamga, S. Aïssa, T. R. Rasethuntsa, and M.-S. Alouini, "Mixed RF/FSO communications with outdated-CSI-based relay selection under double generalized Gamma turbulence, generalized pointing errors, and Nakagami-m fading," *IEEE Trans. Wireless Commun.*, vol. 20, no. 5, pp. 2761–2775, May 2021.

[15] O. B. Yahia, E. Erdogan, G. K. Kurt, I. Altunbas, and H. Yanikomeroglu, "A weather-dependent hybrid RF/FSO satellite communication for improved power efficiency," *IEEE Wireless Commun. Lett.*, vol. 11, no. 3, pp. 573–577, Mar. 2022.

[16] M. V. Jamali and H. Mahdavifar, "Uplink non-orthogonal multiple ieee over mixed RF-FSO systems," *IEEE Trans. Wireless Commun.*, vol. 19, no. 5, pp. 3558–3574, May 2020.

[17] P. Yan, Y. Zou, X. Ding, and J. Zhu, "Energy-aware relay selection improves security-reliability tradeoff in energy harvesting cooperative cognitive radio systems," *IEEE Trans. Veh. Technol.*, vol. 69, no. 5, pp. 5115–5128, May 2020.

[18] B. Li, Y. Zou, J. Zhu, and W. Cao, "Impact of hardware impairment and co-channel interference on security-reliability trade-off for wireless sensor networks," *IEEE Trans. Wireless Commun.*, vol. 20, no. 11, pp. 7011–7025, Nov. 2021.

[19] K. P. Peppas, N. C. Sagias, and A. Maras, "Physical layer security for multiple-antenna systems: A unified approach," *IEEE Trans. Commun.*, vol. 64, no. 1, pp. 314–328, 2015.

[20] S. C. Tokgoz, S. Althunibat, S. L. Miller, and K. A. Qaraqe, "On the secrecy capacity of hybrid FSO-mmwave wiretap channels," *IEEE Trans. Veh. Technol.*, vol. 71, no. 4, pp. 4073–4086, Apr. 2022.

[21] E. Erdogan, I. Altunbas, G. K. Kurt, and H. Yanikomeroglu, "The secrecy comparison of RF and FSO eavesdropping attacks in mixed RF-FSO relay networks," *IEEE Photonics J.*, vol. 14, no. 1, pp. 1–8, Feb. 2021.

[22] D. R. Pattanayak, V. K. Dwivedi, V. Karwal, A. Upadhya, H. Lei, and G. Singh, "Secure transmission for energy efficient parallel mixed FSO/RF system in presence of independent eavesdroppers," *IEEE Photonics J.*, vol. 14, no. 1, pp. 1–14, Feb. 2022.

[23] C. Gong, X. Yue, X. Wang, X. Dai, R. Zou, and M. Essaaidi, "Intelligent reflecting surface aided secure communications for NOMA networks," *IEEE Trans. Veh. Technol.*, vol. 71, no. 3, pp. 2761–2773, Mar. 2021.

[24] P. Yang, L. Yang, and S. Wang, "Performance analysis for RIS-aided wireless systems with imperfect CSI," *9172088IEEE Wireless Commun. Lett.*, vol. 11, no. 3, pp. 588–592, Mar. 2021.

[25] Z. Zhang, J. Chen, Q. Wu, Y. Liu, L. Lv, and X. Su, "Securing NOMA networks by exploiting intelligent reflecting surface," *IEEE Trans. Commun.*, vol. 70, no. 2, pp. 1096–1111, Nov. 2021.

[26] Z. Wei, X. Zhu, S. Sun, and Y. Huang, "Energy-efficiency-oriented cross-layer resource allocation for multiuser full-duplex decode-and-forward indoor relay systems at 60 GHz," *IEEE Journal on Selected Areas in Communications*, vol. 34, no. 12, pp. 3366–3379, Sep. 2016.

[27] S. Zhang, H. Gu, K. Chi, L. Huang, K. Yu, and S. Mumtaz, "Drl-based partial offloading for maximizing sum computation rate of wireless powered mobile edge computing network," *IEEE Trans. Wireless Commun.*, vol. 21, no. 12, pp. 10 934–10 948, 2022.

[28] Y. Ni, Y. Liu, J. Wang, Q. Wang, H. Zhao, and H. Zhu, "Performance analysis for RIS-assisted D2D communication under Nakagami-m fading," *IEEE Trans. Veh. Technol.*, vol. 70, no. 6, pp. 5865–5879, Jun. 2021.

[29] E. Basar, M. Di Renzo, J. De Rosny, M. Debbah, M.-S. Alouini, and R. Zhang, "Wireless communications through reconfigurable intelligent surfaces," *IEEE Access*, vol. 7, pp. 116 753–116 773, Aug. 2019.

[30] B. Ashrafzadeh, E. Soleimani-Nasab, A. Zaimbashi, and M. Uysal, "Outage performance of mixed RF-FSO systems over DGG and Nakagami-m channels," *IEEE Wireless Commun. Lett.*, vol. 9, no. 12, pp. 2135–2139, Dec. 2020.

[31] I. S. Ansari, F. Yilmaz, and M.-S. Alouini, "Performance analysis of free-space optical links over Málaga (M) turbulence channels with pointing errors," *IEEE Trans. Wireless Commun.*, vol. 15, no. 1, pp. 91–102, Jan. 2016.

[32] A. M. Salhab and L. Yang, "Mixed RF/FSO relay networks: RIS-equipped RF source vs RIS-aided RF source," *IEEE Wireless Commun. Lett.*, vol. 10, no. 8, pp. 1712–1716, May 2021.

[33] A. H. Abd El-Malek, A. M. Salhab, S. A. Zummo, and M.-S. Alouini, "Security-reliability trade-off analysis for multiuser simo mixed RF/FSO relay networks with opportunistic user scheduling," *IEEE Trans. Wireless Commun.*, vol. 15, no. 9, pp. 5904–5918, May 2016.

[34] W. Research, "Meijerg function," https://functions.wolfram.com/PDF/MeijerG.pdf.
[35] A. Soulimani, M. Benjillali, H. Chergui, and D. B. da Costa, "On multihop Weibull-fading communications: performance analysis framework and applications," *arXiv preprint arXiv:1610.08535*, 2016.
[36] H. Chergui, M. Benjillali, and S. Saoudi, "Performance analysis of project-and-forward relaying in mixed MIMO-pinhole and Rayleigh dual-hop channel," *IEEE Commun. Lett.*, vol. 20, no. 3, pp. 610–613, 2016.
[37] X. Ding, Y. Zou, G. Zhang, X. Chen, X. Wang, and L. Hanzo, "The security–reliability tradeoff of multiuser scheduling-aided energy harvesting cognitive radio networks," *IEEE Trans. Commun.*, vol. 67, no. 6, pp. 3890–3904, Mar. 2019.
[38] L. Huang, R. Nan, K. Chi, Q. Hua, K. Yu, N. Kumar, and M. Guizani, "Throughput guarantees for multi-cell wireless powered communication networks with non-orthogonal multiple access," *IEEE Trans. Veh. Technol.*, vol. 71, no. 11, pp. 12 104–12 116, 2022.
[39] S. Atapattu, C. Tellambura, and H. Jiang, "A mixture gamma distribution to model the SNR of wireless channels," *IEEE Trans. Wireless Commun.*, vol. 10, no. 12, pp. 4193–4203, 2011.
[40] D. Zwillinger and A. Jeffrey, *Table of integrals, series, and products*. Elsevier, 2007.

Dawei Wang (Member, IEEE) received the B.S. degree from University of Jinan, China, in 2011 and the Ph.D. degree from Xi'an Jiaotong University, China in 2018. From 2016 to 2017, he was a Visiting Student with the School of Engineering, The University of British Columbia. He is currently an Associate Professor with the School of Electronics and Information, Northwestern Polytechnical University, Xi'an, China. He has served as Technical Program Committee (TPC) member for many international conferences, such as IEEE GLOBECOM, IEEE ICC, etc. His research interests include Physical-Layer Security, Cognitive Radio Networks, Machine Learning, NOMA Communications, UAV Communications, and Resource Allocation.

Menghan Wu received the B.S. degree in communication engineering from Northwestern Polytechnical University, Shaanxi, China, in 2021. She is currently working toward the M.E. degree in School of Electronics and Information with Northwestern Polytechnical University, Xi'an, China. Her research interests include UAV communication networks, cooperative relaying, machine learning, and physical-layer security.

Zhongxiang Wei (M'17) (Member, IEEE) received the Ph.D. degree in electrical and electronics engineering from the University of Liverpool, Liverpool, U.K., in 2017.

From March 2016 to March 2017, he was a Research Assistant with the Institution for Infocomm Research, Agency for Science, Technology and Research, Singapore. From March 2018 to March 2021, he was a Research Associate with the Department of Electrical and Electronics Engineering, University College London. He is currently an Associate Professor with the College of Electronic and Information Engineering, Tongji University, China. He has authored or coauthored more than 60 research papers published on top-tier journals and international conferences. His research interests include anonymous communications, constructive interference designs, and millimeter-wave communications. He has acted as a Session/Track Chair or a TPC Member of various international flagship conferences, such as IEEE ICC, GLOBECOM, and ICASSP. He was a recipient of the Shanghai Leading Talent Program (Young Scientist) in 2021, an Exemplary Reviewer of the IEEE TRANSACTIONS ON WIRELESS COMMUNICATIONS in 2016, the Outstanding Self-Financed Students Abroad in 2018, and the A*STAR Research Attachment Program (ARAP) in 2016.

Keping Yu (Member, IEEE) received the M.E. and Ph.D. degrees from the Graduate School of Global Information and Telecommunication Studies, Waseda University, Tokyo, Japan, in 2012 and 2016, respectively. He was a Research Associate, Junior Researcher, Researcher with the Global Information and Telecommunication Institute, Waseda University, from 2015 to 2019, 2019 to 2020, 2020 to 2022, respectively. He is currently an associate professor at Hosei University, Japan.

Dr. Yu has hosted and participated in more than ten projects, is involved in many standardization activities organized by ITU-T and ICNRG of IRTF, and has contributed to ITU-T Standards Y.3071 and Supplement 35. He received the IEEE Outstanding Leadership Award from IEEE BigDataSE 2021, the Best Paper Award from IEEE Consumer Electronics Magazine Award 2022 (1st Place Winner), IEEE ICFTIC 2021, ITU Kaleidoscope 2020, the Student Presentation Award from JSST 2014. He has authored more than 200 peer-review research papers and books, including over 70 IEEE/ACM Transactions papers. He is an Associate Editor of IEEE Open Journal of Vehicular Technology, Journal of Intelligent Manufacturing, Journal of Circuits, Systems and Computers, and IEICE Transactions on Fundamentals of Electronics, Communications and Computer Sciences. He has been a Guest Editor for more than 20 journals such as IEEE Transactions on Computational Social Systems, IEEE Journal of Biomedical and Health Informatics, and Renewable & Sustainable Energy Reviews. He served as general co-chair and publicity co-chair of the IEEE VTC2020-Spring 1st EBTSRA workshop, general co-chair of IEEE ICCC2020 2nd EBTSRA workshop, general co-chair of IEEE TrustCom2021 3nd EBTSRA workshop, session chair of IEEE ICCC2020, ITU Kaleidoscope 2016. His research interests include smart grids, information-centric networking, the Internet of Things, artificial intelligence, blockchain, and information security.

Lingtong Min (Member, IEEE) received the B.S. degree from Northeastern University, Shenyang, China, in 2012, and the Ph.D. degree from Zhejiang University, Hangzhou, China, in 2019. He is currently an Associate Professor with Northwestern Polytechnical University, Xi'an, China. His main research interests include computer vision, pattern recognition, and remote sensing image understanding.

Shahid Mumtaz (Senior Member, IEEE) is currently with the Department of Applied Informatics, Silesia University Technology, and the Department of Engineering, Nottingham Trent University. He has more than 12 years of wireless industry experience. His research interests include architectural enhancements to 3GPP networks, 5G NR related technologies, green communications, cognitive radio, cooperative networking, radio resource management, network slicing, LAA/LTU, cross-layer design, backhaul/fronthaul, heterogeneous networks, M2M and D2D communication, and baseband digital signal processing.